2008 American Control Conference
Westin Seattle Hotel, Seattle, Washington, USA
June 11-13, 2008

AFM Imaging of Large Soft Samples in Liquid Medium Using Iterative Inverse Feedforward Control

Szuchi Tien and Santosh Devasia

Abstract— **A zoom-out/zoom-in iterative method is proposed to maintain small tip-sample forces during high-speed AFM imaging of soft samples in liquid. The method is used to demonstrate high-speed imaging of soft hydrogel samples.**

I. Introduction

The main contribution of this article is the enabling of high-speed AFM imaging of soft samples in liquid while maintaining small tip-sample force. High-speed imaging of soft samples (e.g., biological or polymer samples) with an Atomic Force Microscope (AFM) is challenging because a large tip-sample force can lead to sample damage and tip-contamination. High-speed imaging of such samples in a fluid medium is particularly challenging because fluid effects such as meniscus interactions and viscous damping can make it challenging to control the tip-sample force. Thus, the inability to maintain small tip-sample force at high scan frequencies implies that current AFM imaging of soft samples is slow (with imaging times in the minutes for each frame) especially when imaging relatively large areas (e.g., $10\mu m \times 10\mu m$) of soft samples. However, high-speed AFM is necessary to investigate and manipulate dynamic nanoscale phenomena in applications such as nanofabrication with soft polymers and imaging of soft biological samples. This article proposes a zoom-out/zoom-in iterative method to achieve the precision positioning needed to maintain small tip-sample forces during high-speed AFM imaging. The method is used to demonstrate high-speed imaging of soft hydrogel samples.

Need for Precision-Positioning The tip-sample force depends on the distance between the AFM-probe and the sample surface (i.e., the tip-sample distance). Therefore, the AFM-probe's tip should precisely follow the sample's topography (i.e., the sample profile along each scan line) during the scanning process. This is particularly important with soft samples, because if the probe does not follow the sample profile, then the AFM-probe tip can dig into sample, which can result in excessive tip-sample forces and sample damage. As the scan frequency increases, the AFM-probe's tip has to track the sample's topography faster. Thus, high-speed, precision positioning of the AFM-probe is needed to maintain small tip-sample forces during rapid AFM-imaging of soft samples.

Problem: Scanning-induced vibration During AFM imaging, a piezoscanner positions the tip of the AFM-probe relative to the sample surface in the x-y axes (parallel to sample's substrate) and z axis (perpendicular to the sample's substrate). As the scan frequency is increased relative to the smallest, resonant-vibrational frequency of the piezoscanner, the vibrational modes of the piezoscanner are excited and the resulting vibrations cause errors in the positioning of the AFM-probe over the sample surface. The positioning errors become significant at high scan frequencies; thereby, limiting the maximum operating speed of the AFM.

Scan Size vs. Scan Frequency If a small area is scanned, then the sample profile variation (topography variation along each scan line) is small and the change in AFM-probe position is small. Therefore, when the scan size (i.e., the dimension of each scan line) is small, the vibrations (due to small motions of the piezoscanner) are also small. Hence, small sample areas can be imaged with AFM at relatively high-speeds. For example, high-speed ($80ms$ per frame) AFM imaging over a scan size of $0.24\mu m$ was demonstrated to visualize fast dynamics [1]. Such tradeoffs between imaging speed (scan frequency) and scan size, for soft samples, is shown in Fig. 1. While the acceptable tip-sample force depends on the imaging conditions and sample properties, the general trend is a reduction in the imaging speed with an increase in scan size [2]-[7] — as shown in Fig. 1. In contrast, this article seeks to increase the scan frequency (AFM imaging speed) for soft samples without reducing the maximum scan size.

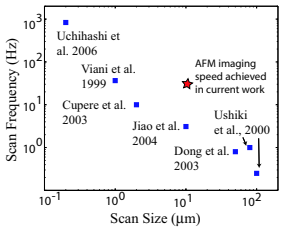

Fig. 1. The tradeoff between scan size and scan frequency for soft samples and the AFM imaging speed (scan frequency and size) achieved in the current article. These include imaging in liquid medium [3]-[7].

Model-based Feedforward The difficulty in precisely positioning the AFM-probe does not arise because the piezoscanner's scan size is smaller at higher scan frequencies. piezoscanners tend to have low damping and therefore, can move the AFM-probe over a large scan area when the scan frequency is high — especially, when the scan frequency is close to the piezoscanner's resonant-vibrational frequencies. Rather, the problem with AFM-probe positioning is the lack of precision at high scan-frequencies. The lack of precision is caused by scanning-induced vibration during fast scanning

S. Tien is with the Mechanical Engineering, National Cheng-Kung University, Tainan 701, Taiwan; Email: sctien@mail.ncku.edu.tw

S. Devasia is with the Mechanical Engineering Department, U. of Washington, Seattle, WA 98195, USA; Email: devasia@u.washington.edu

978-1-4244-2079-7/08/$25.00 ©2008 AACC.

(in addition to other effects such as creep, hysteresis, and dynamics coupling) — see [8] for a recent review on challenges in nanopositioning. Early work showed that model-based inversion methods can be used to find feedforward inputs, which lead to high-speed, precision lateral (x-y axes) positioning in scanning-probe microscopy [9], [10]; recent advances in feedforward implementation are discussed in [11]-[12]. The feedforward input when integrated with feedback techniques [12]-[14] improve the positioning performance of purely feedback approaches, provided the modeling errors are not too large [15].

Problem with Model-based Feedforward: The model-based inversion methods achieve perfect control of the AFM-probe deflection in the absence of modeling errors. However, modeling errors can occur due to day-to-day variations in the operating conditions such as temperature changes, differences in sample properties, aging of the piezos, unmodeled vibrations, and variations in fluid effects as well as coupling between x, y, z axes. When imaging soft samples, such modeling-error caused positioning error can lead to excessive tip-sample force. During repetitive positioning, especially for periodic scanning in the lateral axes, iterative methods can be used to improve the positioning precision as demonstrated in [16]-[18].

Proposed Iterative Feedforward for Vertical Control This article shows that iterative, model-inversion-based techniques [17], [19] (for precision positioning of the AFM-probe) can be used to maintain a small tip-sample force during high-speed AFM imaging of soft samples in liquid medium. Issues in implementing such iterative methods in an AFM, e.g., maintaining small forces during the first step of the iteration process is also addressed using a zoom-out/zoom-in technique, and the approach is illustrated by imaging a soft hydrogel sample.

II. Problem Formulation

The Positioning Problem The goal is to follow the sample topography with the tip of the AFM-probe, which is positioned with a piezoscanner, both parallel to the sample surface (along the x and y-axis) and perpendicular (along the z-axis) to the sample surface as shown in Fig. 2. In particular, the vertical position z (nm) of the AFM-probe's tip (which corresponds to the estimated sample topography) is a combination of the vertical position z_p (nm) of the piezoscanner and the displacement z_d (nm) due to the deflection of the AFM-probe.

$$\begin{aligned} z(t) &= z_p(t) + z_d(t) \\ &= \tfrac{1}{K_p} z_{ps}(t) + \tfrac{1}{K_d} z_{ds}(t) \end{aligned} \tag{1}$$

where K_p and z_{ps} are the gain (Volts/nm) and output (Volts) of an inductive sensor that measures the position z_p of the piezoscanner, K_d and z_{ds} are the gain (Volts/nm) and output (Volts) of an optical sensor that measures the deflection z_d of the AFM-probe, where the datum is considered to be the initial configuration (of z_p, z_d, z) when the AFM-probe is brought into contact with the sample surface with a nominal force F_{nom}. The corresponding nominal AFM-probe deflection $z_{ds,nom}$ is given by

$$F_{nom} = \frac{k}{K_d} z_{ds,nom} \tag{2}$$

where k (pN/nm) is the spring constant of the probe. While a smaller, nominal deflection $z_{ds,nom}$ corresponds to a smaller nominal tip-sample force F_{nom} the nominal deflection $z_{ds,nom}$ should also be sufficiently large to prevent loss of contact with the sample surface due to variations in the AFM-probe deflection during the imaging process.

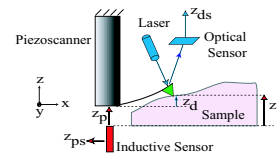

Fig. 2. Schematic of AFM-probe Positioning (not to scale)

The Control Problem The variation of the tip-sample force F (pN) from the nominal value F_{nom} is proportional to the measured AFM-probe deflection z_{ds}, i.e.,

$$F(t) - F_{nom} = k\, z_d(t) = \frac{k}{K_d} z_{ds}. \tag{3}$$

Therefore, the control problem is to reduce deviations from the nominal AFM-probe deflection, i.e., the error $e = 0 - z_{ds}$ by adjusting the vertical position z_p of the piezoscanner as shown in Fig. 3.

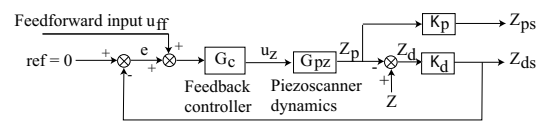

Fig. 3. Feedforward-based scheme to control AFM-probe deflection

Positioning-Error Model The effect of the sample's surface topography z on the error e in the AFM-probe deflection, can be reduced by the choice of the feedforward input u (see Fig. 3). The error dynamics can be modeled as

$$E(\omega) = G_{ff}(\omega) U_{ff}(\omega) + G_z(\omega) Z(\omega) \tag{4}$$

where E, U_{ff} and Z are the Fourier transforms of the following functions in time: AFM-probe-deflection error e, the feedforward input u_{ff}, and the sample topography z. Additionally, ω represents frequency at which the Fourier-domain functions are evaluated, and

$$G_{ff} = \frac{G_c G_{pz} K_d}{1 - G_c G_{pz} K_d}, \qquad G_z = \frac{-K_d}{1 - G_c G_{pz} K_d} \tag{5}$$

where G_{pz} represents the dynamics of the piezoscanner in the vertical direction.

Experimental Modeling Experimental modeling (of the transfer functions G_{ff} and G_z in Eq. 5) is preferred to avoid the challenges of analytically modeling the fluid and contact effects. For example, the dynamics model G_{ff}, of the effect of the feedforward input u_{ff} on the error in the AFM-probe deflection e, can be obtained by using a digital signal analyzer (DSA). Sinusoidal signal generated by the DSA can be applied as input, u_{ff} as in Fig. 3, to the piezoscanner and

the error signal of AFM-probe deflection e can be measured; this input-output data can be used to model the transfer function G_{ff}. Next, G_z can be computed using Eq. 5 as

$$G_z = -K_d\,(1 + G_{ff}). \tag{6}$$

Model-Based Feedforward for Vertical Control The feedforward input U_{ff} can be chosen to account for variations in the deflection error $E(\omega)$ caused by the sample topography $Z(\omega)$ (in Eq. 4), i.e.,

$$G_{ff}(\omega)U_{ff}(\omega) + G_z(\omega)Z(\omega) = 0. \tag{7}$$

Thus, the feedforward input U_{ff} can be found from Eq. (7) by inverting the dynamics G_{ff} as [20]:

$$U_{ff,inv}(\omega) = -G_{ff}^{-1}(\omega)G_z(\omega)Z(\omega). \tag{8}$$

The corresponding time-function $u_{ff,inv}$ can be computed and applied as feedforward input $u_{ff}(t) = u_{ff,inv}(t)$, as shown in the control scheme in Fig. 3.

Iterative Approach to Correct Modeling Errors The inverse input achieves perfect control of the AFM-probe deflection ($e = 0$) in the absence of modeling errors and if the sample topography (Z in Eq. 8) is known. However, modeling errors tend to be unavoidable! More critically, the sample topography Z (in Eq. 8), needed to compute the feedforward input, is unknown. Therefore, an iterative approach is proposed to find the feedforward input. The iterative control law uses the measured error e_k in the AFM-probe deflection during one iteration step k to update the current input from one iteration step k to another $k+1$, i.e., from input $u_{ff,k}$ to input $u_{ff,k+1}$, as

$$U_{ff,k+1}(\omega) = U_{ff,k}(\omega) + \rho(\omega)G_{ff}^{-1}(\omega)\left[E_k(\omega)\right]. \tag{9}$$

In such a scheme, the initial input $U_{ff,0}$ can be chosen as zero. Therefore, the sample topography is not required in the computation of the iterative inputs; rather the algorithm only requires the measured error e_k at each iteration step. The convergence of such iterative control laws, in the presence of modeling errors, has been studied in [17], [19].

Problem: Large Forces During Iterations The problem is to avoid large tip-sample forces (and potential sample damage) during the iteration process and, in particular, during the very first step in the iteration process. One approach, to avoid such sample damage, is to achieve small positioning errors in the first iteration by using feedforward input. For example, a slow scan can be used to identify the sample profile at the start of the iteration process and then the inversion procedure can be used to find the feedforward input for the first iteration. The problem is that this slow scan can take a very long time to begin with and moreover, the sample profile could change during this initial slow scan and therefore, the initial estimate of the sample profile would not be sufficiently accurate for the next iteration.

Proposed Approach: Zoom-out/Zoom-in Iterations The zoom-out/zoom-in approach has three phases as shown in Fig. 4. At the start, the scan size is small. Therefore, the sample-profile variations are small; the resulting positioning errors and the tip-sample forces are also small! The rate at which the scan size is changed during the expansion and reduction phases are adjusted to ensure that the variations in the tip-sample force are small. This gradual increase in scan size to reduce tip-sample force (i.e., change in sample profile between iteration steps) is similar to the concept of using the piezoscanner input when scanning one line of the sample as the initial input for the next line on the sample to reduce tip-sample forces [17], [18].

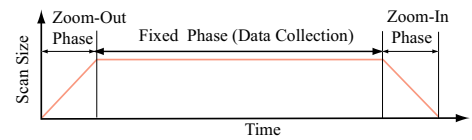

Fig. 4. The three scanning phases (zoom-out phase, fixed phase, and zoom-in phase) to maintain small tip-sample forces during the iteration process.

III. Results for Single Line Scanning

In this section, experimental results, when scanning a single line of a hydrogel sample (shown in Fig. 5), are presented to evaluate: (a) the ability to achieve fast scanning with a small tip-sample force; and (b) the effect of scan frequency on the acquired surface-topography data. The zoom-out/zoom-in approach was not used for iterations in these single-line evaluations; it is considered in the next section.

A. Experimental Conditions

Choice of Soft Sample Hydrogel contact lenses are soft — they have a relatively-small elastic modulus, which tends to be less than 0.5 MPa [21]). Therefore, AFM scanning was performed on soft contact lens samples (1-Day Acuvue, Johnson & Johnson) in saline solution. Moreover, since positioning is relatively challenging over large scan areas and over large variations in sample topography, the scan size was chosen to be ($10\mu m$) and the sample topography variation over this scan size was $1\mu m$ as shown in Fig. 5. This relatively-large sample topography was obtained by tilting the sample surface, which also allowed the comparison of a similar topography over different experiments performed at different times. Typical nanoscale details of the sample surface are shown in Fig. 5, which was obtained by using a standard image-flattening approach [22], i.e., the main surface topography z was fitted with a quadratic polynomial; next, the quadratic polynomial was subtracted from the surface topography z to reveal the nanoscale surface details (also, referred to as the flattened surface z_f).

AFM Operating Conditions The AFM (Molecular Imaging, PicoSPM II) was operated in the contact mode, with a soft silicon nitride AFM-probe (MLCT-NO, Veeco) that had a rated spring constant of $k = 10pN/nm$ = $0.01N/m$. Additional details of operating conditions are described in [23].

Choice of Scan Trajectory To enable comparative evaluation, the scan trajectory was kept the same for the high and low frequency scans. In particular, a high-frequency (ΩHz) sinusoidal input u_x (pre-filtered with a $200Hz$ low-pass filter to avoid coupling effects) was applied to the piezoscanner and the resulting high-frequency movement $x_\Omega(t)$ in the

scan direction was measured, e.g. see Fig. 6. The measured position x_Ω was used as a reference signal $x_{ref,0.5}$ to be followed using feedback during the low-frequency ($0.5Hz$) scanning, where $x_{ref,0.5}(t) = x_\Omega(0.5t/\Omega)$. The achieved low frequency position $x_{0.5}$ tracked the desired scan profile $x_{ref,0.5}$ with high precision; the tracking error was about $20nm$ over the relatively-large $10\mu m$ scan, see Fig. 6.

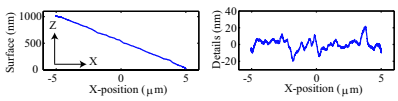

Fig. 5. Typical cross-section (z, left plot) of sample surface and nanoscale details in the flattened surface (z_f right plot) of the surface. Images were obtained at a scan frequency of $0.5Hz$. The scan direction is denoted by x and the vertical position (estimated sample surface) is z in Eq. (1)

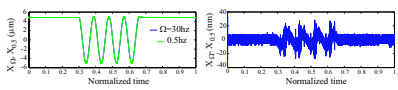

Fig. 6. Left Plot: Comparison of scan trajectory in x-axis at high $\Omega = 30Hz$ and low $0.5Hz$ scan frequencies (measured data). The difference between the two scan trajectories is shown in the right plot.

B. Comparison of Tip-Sample Force

The tip-sample force of the low-frequency $0.5Hz$ scan is compared with that of the high-frequency scans ($\Omega = 20Hz$, and $30Hz$) for three cases: (i) without feedforward $u_{ff} = 0$; (ii) with inverse feedforward $u_{ff,inv}$ (from Eq. 8); and (iii) with iterative feedforward $U_{ff,k}$ (from Eq. 9).

Computational Issues The inverse feedforward input $u_{ff,inv}$, without iteration, requires prior knowledge of the desired vertical position z (see Eq. 8. As discussed before, the desired vertical position (i.e., the sample profile) is unknown before the imaging. However, for comparatively evaluating the benefits of feedforward, with and without iteration, the inverse feedforward was computed using the sample profile estimated with the low frequency scan. For example, to compute the inverse feedforward input $u_{ff} = U_{ff,inv,\Omega}$ at a scan frequency of ΩHz, an estimate of the surface topography z_Ω during high-speed scanning was estimated from the low-frequency measurements of the surface topography $z_{0.5}$ as

$$z_\Omega(t) = z_{0.5}(\Omega\ t/0.5). \tag{10}$$

Next, the inverse feedforward input $U_{ff,inv,\Omega}$ was computed in the frequency domain as in Eq. 8

$$\begin{aligned} U_{ff,inv,\Omega}(\omega) &= -G_{ff}^{-1}(\omega)G_z(\omega)Z_\Omega(\omega) \quad \forall\omega \le 10\Omega \\ &= 0 \quad \forall\omega > 10\Omega. \end{aligned} \tag{11}$$

Setting the inverse input to zero, $U_{ff,inv,\Omega}(\omega) = 0$, at frequencies $\omega > 10\Omega$ filtered noise in the measured data. Similarly, during each step of the iteration process, a frequency domain filtering was used to compute the iterative feedforward $u_{ff} = U_{ff,k+1,\Omega}$ in Eq. (9) by choosing

$$\begin{aligned} \rho &= 0.2 \quad \text{if } \omega \le 10\Omega \\ &= 0 \quad \text{if } \omega > 10\Omega \end{aligned} \tag{12}$$

and the inverse input $u_{ff,inv,\Omega}$ as the initial input.

Tip-Sample Force Increases with Scan Frequency The tip-sample force tends to become large as scan frequency increases (when feedforward is not used) as seen in the first two rows of Table I, which shows data for $20Hz$ and $30Hz$ — additional data is available in [23]. During low-frequency scanning of $0.5Hz$, the control system maintained the average tip-sample force $\bar{F}$ close to the desired (nominal) value of $150pN$. The corresponding standard deviation σ_F for this low-frequency reference scan was less than $30pN$ when the AFM-probe was actively scanning over the sample surface, e.g., during the normalized time interval $[0.295, 0.659]$ in Fig. 6. Moreover, the maximum value F_{max} of the tip-sample force was less than $300pN$ without the use of feedforward input, see first row of Table I. However, as the scan frequency was increased, the maximum tip-sample force F_{max} increased significantly without the inverse input $u_{ff} = 0$. In particular, the maximum force F_{max} increased to more than $2000pN$ at $30Hz$ scan frequency, as shown in the second row of Table I.

TABLE I

COMPARISON OF TIP-SAMPLE FORCE F (PN)

	20Hz			30Hz		
	$\bar{F}$	σ_F	F_{max}	$\bar{F}$	σ_F	F_{max}
0.5Hz	149.9	24.6	229.0	150.1	24.8	232.7
$u_{ff} = 0$	219.1	491.7	1538.2	272.2	563.7	2172.5
$u_{ff,inv,\Omega}$	124.2	138.6	414.2	111.8	115.6	371.2
$u_{ff,k,\Omega}$	143.7	57.6	268.7	148.5	28.6	226.3
k		10			30	
Noise†	22.5	18.5	100.4	7.0	5.8	44.6

†Noise is the non-repeatability in tip-sample force between two consecutive scans with the same feedforward input $u_{ff,inv,\Omega}$ [23].

Inverse Feedforward Reduces Tip-Sample Force This reduction is compared in the second and third rows of Table I. In particular, the maximum tip-sample force F_{max} was reduced from $2173pN$ to $371pN$ at a relatively-high scan frequency of $30Hz$ with the use of the inversion-based feedforward input. The reduction in the tip-sample force at higher scan frequencies is achieved by adjusting the vertical position of the AFM-probe to follow the sample topography. To illustrate this, the feedforward input u_{ff} and the vertical position of the piezoscanner z_p for the $30Hz$ scan frequency are shown in Fig. 7, with and without the inverse feedforward input. Without the inverse feedforward input $u_{ff} = 0$, the vertical position of the piezoscanner z_p (Fig. 7, solid line in the right plot) is not similar to the typical sample topography, which changes by a micron during the scan (shown in Fig. 5).

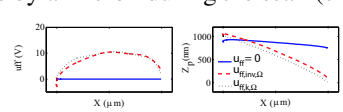

Fig. 7. Feedforward input u_{ff} and vertical position z_p of piezoscanner at high scan frequency, $\Omega = 30Hz$: without inverse feedforward input ($u_{ff} = 0$, solid line); with inverse feedforward ($u_{ff} = u_{ff,inv,\Omega}$, dashed line); and with iterative-inverse-feedforward input at the final iteration ($u_{ff} = u_{ff,k,\Omega}$, dotted line).

This implies, that the tip-sample force can be substantially large because the AFM-probe's tip has to deflect substantially

when following the sample topography. On the other hand, with the inverse feedforward input, the vertical position of the piezoscanner z_p is close to the sample topography — compare dashed line in right plot of Fig. 7 with the sample topography in Fig. 5. Thus, the AFM-probe's tip does not have to deflect substantially to follow the sample topography, and therefore, the tip-sample force is substantially reduced.

Results with Iterative Approach The use of the iterative feedforward $u_{ff,k,\Omega}$ leads to further reduction in the tip-sample force when compared to the use of the inverse feedforward input — compare rows three and four in Table I. In particular, the maximum tip-sample force F_{max} was reduced to $226pN$ at the relatively-high scan frequency of $30Hz$ with the use of the iterative input. In contrast, the maximum tip-sample force was $371pN$ with the use of the inverse feedforward input and $2173pN$ without the feedforward input. Again, this reduction in the tip-sample force is achieved by modifying the feedforward input such that the vertical position of the piezoscanner z_p is closer to the sample topography — see dotted lines in Fig. 7.

Limits of Improvement with Iterations Noise (or non-repeatability, see row five of Table I) presents a limit on the maximum reduction of the tip-sample force. For example, the maximum variation in the tip-sample force at $30Hz$ is $45pN$. Then, the anticipated reduction in tip-sample force (over all possible choices of iteration gains [17]) can be estimated as the sum of this variation ($45pN$) and the nominal value ($150pN$) of the tip-sample force, i.e., $195pN$. The maximum value of the tip-sample force (at the final iteration) is $226pN$, which is close to the estimated lowest value, $195pN$.

C. Comparison of Surface Topography

This section evaluates the effect of increasing the scan frequency Ω on the measured surface topography z by comparing the high-scan-frequency surface topography z_Ω with the reference surface topography $z_{0.5}$ estimated at the relatively low scan frequency of $0.5Hz$.

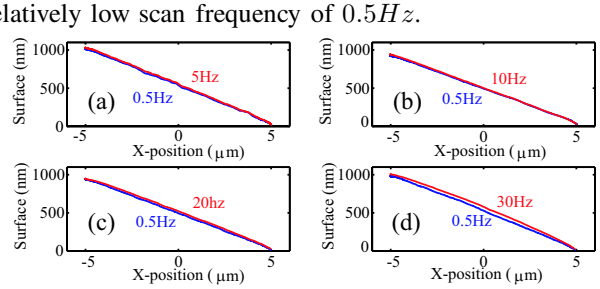

Fig. 8. Comparison of the estimated surface z_Ω at the high scan frequency Ω with the reference surface $z_{0.5}$ at the low scan frequency of $0.5Hz$: (a) $\Omega = 5Hz$; (b) $\Omega = 10Hz$; (c) $\Omega = 20Hz$; (d) $\Omega = 30Hz$.

Results: Measured Surface Topography The surface z was estimated using the measured position z_p of the piezoscanner and the deflection z_d of the piezoscanner (see, Eq. 1). At each scan frequency Ω, data from the four scans in the same scan direction (from $-5\mu m$ to $5\mu m$, see Fig. 6 for the scan profile) are averaged to obtain the AFM-probe's tip position z_Ω. The estimated surface z_Ω at the high scan frequency is compared with the estimated surface $z_{0.5}$ at the low scan frequency of $0.5Hz$ in Fig. 8.

Results: Flattened Surface Topography To compare the nanoscale features over this relatively large scan size of $10\mu m$, flattened data $z_{f,\Omega}$ were obtained by removing larger scale features, as discussed before. The flattened surface $z_{f,\Omega}$ at the high scan frequency is compared with the flattened surface $z_{f,0.5}$ at the low scan frequency of $0.5Hz$ in Fig. 9.

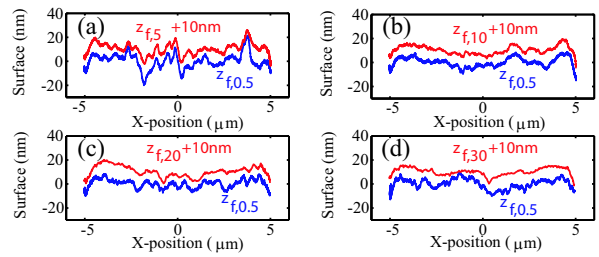

Fig. 9. Comparison the flattened surface $z_{f,\Omega}$ at the high scan frequency Ω with the flattened, reference surface $z_{f,0.5}$ at the low scan frequency of $0.5Hz$: (a) $\Omega = 5Hz$; (b) $\Omega = 10Hz$; (c) $\Omega = 20Hz$; (d) $\Omega = 30Hz$.

Scan Frequency Effects on Surface Topography The estimated surfaces at the higher scan frequency (z_Ω and $z_{f,\Omega}$) are similar to the reference surfaces ($z_{0.5}$ and $z_{f,0.5}$) estimated with a lower-scan frequency as seen in Figures 8 and 9. The change in estimated surface e_z and flattened surface e_{zf} are quantified as

$$e_z = \max_{x\in[-5\mu m, 5\mu m]} |z_\Omega - z_{0.5}|$$
$$e_{zf} = \max_{x\in[-5\mu m, 5\mu m]} |z_{f,\Omega} - z_{f,0.5}|$$

and presented in Table II.

TABLE II
CHANGE IN MEASURED TOPOGRAPHY (e_z, e_{zf} *in nm*)

Surface	5Hz	10Hz	20Hz	30Hz
e_z	27.0	18.7	29.9	55.1
Noise	13.8	6.0	8.9	12.5
Flattened-surface	5Hz	10Hz	20Hz	30Hz
e_{zf}	8.4	6.8	6.5	9.6
Noise	13.9	5.5	5.9	10.4

Surface Topography Error is Small Noise limits the ability to estimate the sample features even at the low, reference scan frequency of $0.5Hz$. The noise is quantified as the non-repeatability in the estimated surfaces ($z_{0.5}$ and $z_{f,0.5}$) in two consecutive scans performed at $0.5Hz$ and presented in Table II. Nanoscale features are still captured by the high-frequency scans. For example, at each scan frequency, the maximum error in the flattened images is close to the noise in the flattened reference images — compare the last two rows in Table II. Moreover, the maximum error in the overall surface of $55nm$ (at $30Hz$ in Table II), which is larger than the noise level (more systematic error) is still less than 6% of the overall height variation of $1\mu m$ in the sample topography.

IV. Results with Zoom-out/Zoom-in Approach

In this section, we present AFM-imaging results with the zoom-out/zoom-in approach for soft hydrogel samples. The

experimentally obtained bode plot of the feedforward transfer function G_{ff} was fitted with a model $\hat{G}_{ff}$, which was used to compute the inverse transfer function G_{inv} as

$$\begin{aligned} G_{inv}(\omega) &= [\hat{G}_{ff}(\omega)]^{-1} \quad \text{if } \omega \leq 300Hz \\ &= 0 \quad \text{otherwise .} \end{aligned} \tag{13}$$

Note that the inverse is set to zero at frequencies greater than ten times the maximum scan frequency ($30Hz$) considered in this work. The time domain representation g_{inv} of the inverse transfer function $G_{inv}(\omega)$, obtained using the inverse Fourier transform, was used in the following time domain version of the frequency-domain iterative control law (in Eq. 9)

$$u_{ff,k+1}(t) = u_{ff,k}(t) \ + \rho \int_{t-T_{review}}^{t+T_{preview}} g_{inv}(\tau) e_k(t-\tau) d\tau. \tag{14}$$

See [23] for additional implementation details.

AFM Imaging Results High-speed AFM scanning of large hydrogel samples in liquid medium was achieved with small forces as shown in Fig. 10 and Fig. 11. Additionally, data for two consecutive scans was collected and the difference was used to quantify the non-repeatable (noise) component in the tip-sample force and shown in Fig. 11. The maximum tip-sample force is less than $500pN$ (obtained by including the nominal force of $200pN$) which is considered small even for imaging extremely soft samples like living cells. Our ongoing efforts are focused on implementing this algorithm for imaging of such soft cell samples.

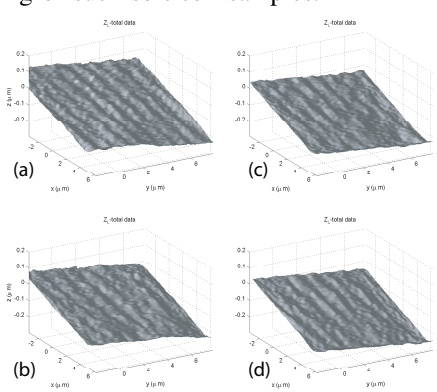

Fig. 10. The topographies measured at different scanning frequency: (a)1Hz (only feedback), (b)10Hz, (c)20Hz, (d)30Hz.

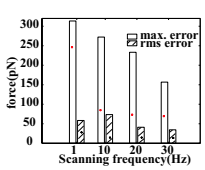

Fig. 11. Force reduction with iterative approach. ('*' indicates the non-repeatable component in the force).

V. Conclusions

A zoom-out/zoom-in iterative method was proposed to achieve small tip-sample forces during high-speed Atomic Force Microscope imaging of soft samples in liquid medium. The method was used to demonstrate high-speed imaging of soft hydrogel samples.

VI. Acknowledgments

Support from NIH Grant GM68103 and NSF Grant CMS 0301787 are gratefully acknowledged.

References

[1] T. Ando, N. Kodera, E. Takai, D. Maruyama, K. Saito, and A. Toda. A high-speed atomic force microscope for studying biological macromolecules. *Proceedings of the National Academy of Sciences of the USA*, 98(22):12468–12472, Oct., 2001.

[2] T. Uchihashi, N. Kodera, H. Itoh, H. Yamashita, and T. Ando. Feed-forward compensation for high-speed atomic force microscopy imaging of biomolecules. *Japanese Journal of Applied Physics*, 45(3B):1904–1908, 2006.

[3] H. Dong, M. Wanyun, L. Fulong, Y. Meiling, O. Zhigang, and S. Yunxu. Time-series observation of the spreading out of microvessel endothelial cells with atomic force microscopy. *Physics in Medicine and Biology*, 48:3897–3909, 2003.

[4] T. Ushiki, S. Yamamoto, J. Hitomi, S. Ogura, T. Umemoto, and M. Shigeno. Atomic force microscopy of living cells. *Japanese Journal of Applied Physics*, Part 1(6B):3761–3764, 2000.

[5] M. B. Viani et. al. Fast imaging and fast force spectroscopy of single biopolymers with a new atomic force microscope desinged for small cantilever. *Rev. of Scientific Instruments*, 70(11):4300–4303, 1999.

[6] Y. Jiao and T. E. Schäffer. Accurate height and volume measurements on soft samples with the atomic force microscope. *Langmuir*, 20:10038–10045, 2004.

[7] V. M. D. Cupere, J. V. Wetter, and P. G. Rouxhet. Nanoscale organization of collagen and mixed collagen-pluronic adsorbed layers. *Langmuir*, 19:6957–6967, 2003.

[8] S. Devasia, E. Eleftheriou, and S. O. Reza Moheimani. A survey of control issues in nanopositioning. *IEEE Transactions on Control Systems Technology*, 15(5):802–823, Sept, 2007.

[9] D. Croft and S. Devasia. Vibration compensation for high speed scanning tunneling microscopy. *Review of Scientific Instruments*, 70(12):4600–4605, Dec. 1999.

[10] D. Croft, G. Shedd, and S. Devasia. Creep, hysteresis, and vibration compensation for piezoactuators: Atomic force microscopy application. *J. of Dyn. Sys., Meas. and Control*, 123(35):35–43, March, 2001.

[11] Yang Li and John Bechhoefer. Feedforward control of a closed-loop piezoelectric translation stage for atomic force microscope. *Review of Scientific Instruments*, 78, 013702:1–8, January, 2007.

[12] Q. Zou, K. K. Leang, E. Sadoun, M. J. Reed, and S. Devasia. Control issues in high-speed afm for biological applications: Collagen imaging example. *Special Issue on* Advances in Nano-technology Control, *Asian Journal Control*, 6(2):164–178, June 2004.

[13] G. Schitter, P. Menold, H. F. Knapp, F. Allgöwer, and A. Stemmer. High performance feedback for fast scanning atomic force microscopes. *Review of Scientific Instruments*, 72(8):3320–3327, 2001.

[14] S. Salapaka, A. Sebastian, J. P. Cleveland, and M. V. Salapaka. High bandwidth nano-positioner: A robust control approach. *Review of Scientific Instruments*, 73(9):3232–3241, Sept., 2002.

[15] S. Devasia. Should model-based inverse input be used as feedforward under plant uncertainty? *IEEE Trans. on Automatic Control*, 47(11):1865–1871, Nov. 2002.

[16] G. M. Clayton and S. Devasia. Iterative image-based modeling and control for higher scanning probe microscope performance. *Review of Scientific Instruments*, 78(8):Article No. 083704, 2007.

[17] S. Tien, Q. Zou, and S. Devasia. Iterative control of dynamics-coupling-caused errors in piezoscanners during high-speed AFM operation. *IEEE Tran. on Cont. Sys. Tech.*, 13(6):921–931, 2005.

[18] G. Schitter, F. Allgöwer, and A. Stemmer. A new control strategy for high-speed atomic force microscopy. *Nanotech.*, 15:108–114, 2004.

[19] J. Ghosh and B. Paden. Iterative learning control for nonlinear nonminimum phase plants. *J. of Dyn. Sys., Meas. and Control*, 123:21–30, March, 2001.

[20] E. Bayo. A finite-element approach to control the end-point motion of a single-link flexible robot. *J. of Robotic Sys.*, 4(1):63–75, 1987.

[21] Eric Papas. Elastic modulus and silicone hydrogels contact lens fitting. *Silicone Hydrogels*, 23, Aug. 2005.

[22] H. Edwards. New method to estimate step heights in scanning-probe microscope images. *Nanotechnology*, 8(1):6–9, March, 1997.

[23] S. Tien. High-speed nano-precision positioning: Theory and applicaiton to AFM imaging of soft samples. *PhD Thesis, U. of Washington*, 2007.